Tampere University

Joona Salonen

LOW-TEMPERATURE PHOTOLUMINESCENCE OF (ALUMINUM) GALLIUM ANTIMONIDE

Bachelor's Thesis
Faculty of Engineering and Natural Sciences
Examiners: Dr. Teemu Hakkarainen
May 2025

ABSTRACT

Joona Salonen: Low-temperature photoluminescence of (aluminum) gallium antimonide
Bachelor's Thesis
Tampere University
Bachelor's Programme in Engineering and Natural Sciences
May 2025

Low-temperature photoluminescence (LT-PL) is a phenomenon in which a material emits light due to an impinging photonic flux. This concept can be implemented in many ways to investigate the properties of molecular beam epitaxially (MBE) grown semiconductor devices, hence providing an essential tool in the field of optoelectronic research. Moreover, LT-PL can reveal different defects that form in such devices, thus giving insight into the quality of the device and providing crucial information in the optimization of MBE. The cryogenic conditions enhance the ability to identify these defects by narrowing spectral linewidth as well as revealing phonon replicas which would not be observed in modest temperatures. In this thesis, LT-PL was used to analyze different transitions in metamorphically MBE grown bulk (aluminum) gallium antimonide (AlGaSb).

This thesis first covers the phenomena essential for measuring the LT-PL spectra of bulk samples: band structure formation, band gap composition and temperature dependence, excitons, photoluminescence in bulk III-V semiconductors, optical phonons, defects, and recombination mechanisms. From these subjects, theories of defects and phonon replicas rise as the most crucial ones due to their presence in LT-PL.

Four metamorphically on Si-GaAs grown bulk MBE samples with different structures were measured: 1) a GaSb sample, 2) a low-temperature no-capping-layer $\mathrm{Al_{0.3}Ga_{0.7}Sb}$ sample, 3) a low-temperature capped $\mathrm{Al_{0.3}Ga_{0.7}Sb}$ sample and 4) a high-temperature capped $\mathrm{Al_{0.3}Ga_{0.7}Sb}$ sample. The latter three had a distributed bragg reflector to improve the intensity of the LT-PL peaks. The bulks of the samples were grown in different temperatures: First sample bulk was grown at 500 °C, second at 395 °C, third at 395 °C and the fourth at 530 °C.

The LT-PL measurements revealed different defect states in bulk (aluminum) gallium antimonide. By comparing the PL peaks with literature, defects states belonging to native defects at around 1.13 eV, phonon replicas at 1.11 eV, oxygen at around 1.00 eV, and GaSb band-to-band transition at 0.850 eV were identified. Moreover, growth temperature increased the intensity of the native defect peak and decreased the intensity of the oxygen peak, proving that the growth temperature has a substantial effect on the LT-PL of AlGaSb devices.

Keywords: LT-PL, Native defects, Phonon replicas, MBE, Telecommunications

TIIVISTELMÄ

Joona Salonen: Matalan lämpötilan fotoluminisenssi (alumiini)galliumantimonidissa
Kandidaatintyö
Tampereen yliopisto
Tekniikan ja Luonnontieteiden kandidaatinohjelma
Toukokuu 2025

Matalan lämpötilan fotoluminisenssi (LT-PL, eng. *low-temperature photoluminescence*) on ilmiö, jossa materiaali emittoi valoa pintaansa kohdistuvan fotonivuon seurauksena. Tätä konseptia voidaan hyödyntää monella tavalla molekyylisuihkuepitaksillisesti (MBE, eng. *molecular beam epitaxy*) kasvatettujen puolijohdelaitteiden ominaisuuksien tutkimisessa. Siten tämä ilmiö tarjoaa tärkeän työkalun optoelektronisten laitteiden tutkimiseen ja niiden kasvatusmenetelmien optimoimiseen. Matalan lämpötilan tarkoitus on parantaa defektien tunnistuskykyä kaventamalla spektristä viivanleveyttä sekä paljastaa fononireplikat, joita ei havaita korkeammissa lämpötiloissa. Tässä kandidaatintyössä, LT-PL:ää käytettiin analysoimaan erilaisia energiasiirtymiä metamorfisesti MBE kasvatetuissa bulkki-(alumiini)galliumantimonidi (AlGaSb) näytteissä.

Tämän työn aluksi esitellään fotoluminisenssiin liittyvät perustavanlaatuiset ilmiöt: vyörakenteen muodostuminen, vyöaukon kompositio- ja lämpötilariippuvuus, eksitonit, bulkki-III–V-puolijohteiden fotoluminisenssi, optiset fononit, defektit sekä rekombinaatiomekanismit. Näistä aihealueista defektit ja fononireplikat nousevat tärkeimmiksi, sillä niiden vaikutus LT-PL spektriin on työssä suurin.

Neljä rakenteellisesti eroavaa metamorfisesti Si-GaAs:in päälle MBE kasvatettua bulkkinäytettä mitattiin tässä työssä: 1) GaSb-näyte, 2) matalan lämpötilan päällystämätön $\mathrm{Al_{0.3}Ga_{0.7}Sb}$-näyte, 3) matalan lämpötilan päällystetty $\mathrm{Al_{0.3}Ga_{0.7}Sb}$-näyte ja 4) korkean lämpötilan päällystetty $\mathrm{Al_{0.3}Ga_{0.7}Sb}$-näyte. Kolmessa jälkimmäisessä näytteessä oli hajautetut Bragg peilit (DBR, eng. *distributed bragg reflector*), joiden tarkoituksena oli parantaa LT-PL piikkien intensiteettiä. Näytteiden bulkit kasvatettiin eri lämpötiloissa: ensimmäinen näyte 500 celsiusasteessa, toinen 395 celsiusasteessa, kolmas 395 celsiusasteessa ja neljäs 530 celsiusasteessa.

LT-PL mittaukset paljastivat eri defektitiloja bulkki-AlGaSb:ssa. Vertaamalla piikkien energioita kirjallisuudesta löytyviin arvoihin energiasiirtymät, jotka kuuluivat natiividefekteille 1.13 eV:ssa, fononireplikoille 1.11 eV:ssa, hapelle 1.00 eV:ssa ja GaSb vyöltä-vyölle siirtymille 0.850 eV:ssa, tunnistettiin. Tämän lisäksi kasvatuslämpötilan huomattiin kasvattavan natiividefektien konsentraatiota ja vähentävän hapen konsentraatiota, mikä osoittaa, että kasvatuslämpötilalla on erittäin suuri merkitys AlGaSb-pohjaisten puolijohdelaitteiden toimintaan.

Avainsanat: LT-PL, Natiivi defektit, Fononi replikat, MBE, Telekommunikaatio

USE OF ARTIFICIAL INTELLIGENCE IN THIS WORK

Artificial intelligence (AI) has been used in generating this work:

☐ No
☒ Yes

I hereby declare, that the AI-based applications used in generating this work are as follows:

Application	**Version**
ChatGPT	4o
Scopus AI	(10.4.2025)
Writefull	(10.4.2025)

Purpose of the use of AI

ChatGPT was used to fix errors in the LaTex project code. Scopus AI was used to quick search for possible sources. Writefull was used to check for typos in the text.

Parts of this work, where AI was used

ChatGPT was not used in any part of the text. Writefull was used in the entire text. Sources 16, 17, 28 and 29 were found with the help of Scopus AI.

Acknowledgement of risks

I hereby acknowledge, that as the author of this work, I am fully responsible for the contents presented in this thesis. This includes the parts that were generated by an AI, in part or in their entirety. I therefore also acknowledge my responsibility in the case, where use of AI has resulted in ethical guidelines being breached.

CONTENTS

LIST OF FIGURES

1. INTRODUCTION

Photoluminescence is a phenomenon in which a material emits photons upon being exposed to a light source [1]. Therefore, controlling the properties of the material allows the tuning of wavelength and the control of carrier flow, resulting in the realization of many applications in photonic integrated circuits and high-speed telecommunications [2].

In recent years, an increasing amount of information has been sent via optical fibers. These optical single-mode fibers have their minimum attenuation at $1550\,\mathrm{nm}$ [2, 3], thus the demand for semiconductor devices, which operate at such wavelengths, has grown. As such, aluminum-gallium-antimonide (AlGaSb) semiconductor devices have risen as a possible contender having a wide wavelength tunability [4], the possibility for high-speed operation [5], and a suitable existing substrate platform. Furthermore, the demands set by bandwidth and portability require technologies that can perform at higher frequencies and operate at lower power, both of which can be achieved with GaSb-based technologies [6]. Still, many challenges remain in the fabrication of AlGaSb-based devices due to defects [2, 7, 8].

This thesis has two goals. The first goal is to identify different recombination mechanisms in metamorphically molecular beam epitaxially (MBE) grown bulk AlGaSb of different compositions using low-temperature photoluminescence (LT-PL) and reveal possible defects that may occur in such devices. The cryogenic conditions act as a means to identify additional recombination mechanisms, e.g., phonon replicas, which would not be observed at modest temperatures. The second goal is to observe the effects of growth temperature on native defect and impurity concentrations, and hence realize more optimal growth conditions for AlGaSb bulk devices.

In Chapter 2, the core theoretical phenomena surrounding III-V semiconductor photoluminescence are discussed. Moving onto Chapter 3, the LT-PL setup, samples, and methods are covered. Then, in Chapter 4, different emission regimes are identified from the LT-PL data. Lastly, in Chapter 5, important results and concepts are summarized.

2. THEORY

This chapter covers in detail the different physical phenomena surrounding semiconductor photoluminescence (PL). First, the formation of band structure in a III-V semiconductor is considered according to the tight binding model (TBM), followed by different parameters that may ultimately affect the band structure. Afterward, excitons and the basic principles of photoluminescence in bulk III-V semiconductors are covered. Lastly, optical phonons, defects, and different recombination mechanisms are considered.

2.1 Band Structure of III-V Semiconductors

In III-V semiconductors, energy bands are formed when group III and V elements come together, forming a zinc-blende structure. This crystalline structure is periodic in nature, and therefore an electron traveling through such a medium is subjected to a periodic background potential. In turn, the periodic background potential is described by a Schrödinger equation appropriate for the semiconductor. The solution for the energy levels of the semiconductor may then be acquired using, e.g., TBM [9], yielding two sets of continuous bands separated by a forbidden zone, called the band gap. In rising energy order, these bands are called the valence and the conduction bands. The valence bands can be further divided into three subbands: 1) Heavy-hole, 2) light-hole, and 3) split-off band. [10]

According to Bloch's theorem, the wave function of an electron is different depending on the lattice periodicity, and therefore the band structure changes with the change of lattice direction. The wave function describing the electron in a periodic potential is

$$\psi_{\boldsymbol{k}} = e^{i\boldsymbol{k}\cdot\boldsymbol{r}} u_{\boldsymbol{k}}, \tag{2.1}$$

where $\boldsymbol{k}$ is the wave-vector, $\boldsymbol{r}$ is the traveling direction of the plane wave describing the electron and $u_{\boldsymbol{k}}$ is a function with the same periodicity as the periodic potential. [9, 11]

Since the wave function depends on the symmetry of the crystal, it is useful to graph energies for different lattice directions in what is known as a dispersion relation. Such a graph then gives insight on whether the semiconductor is direct or indirect, meaning whether the global minimum of the conduction band is aligned with the valence band or

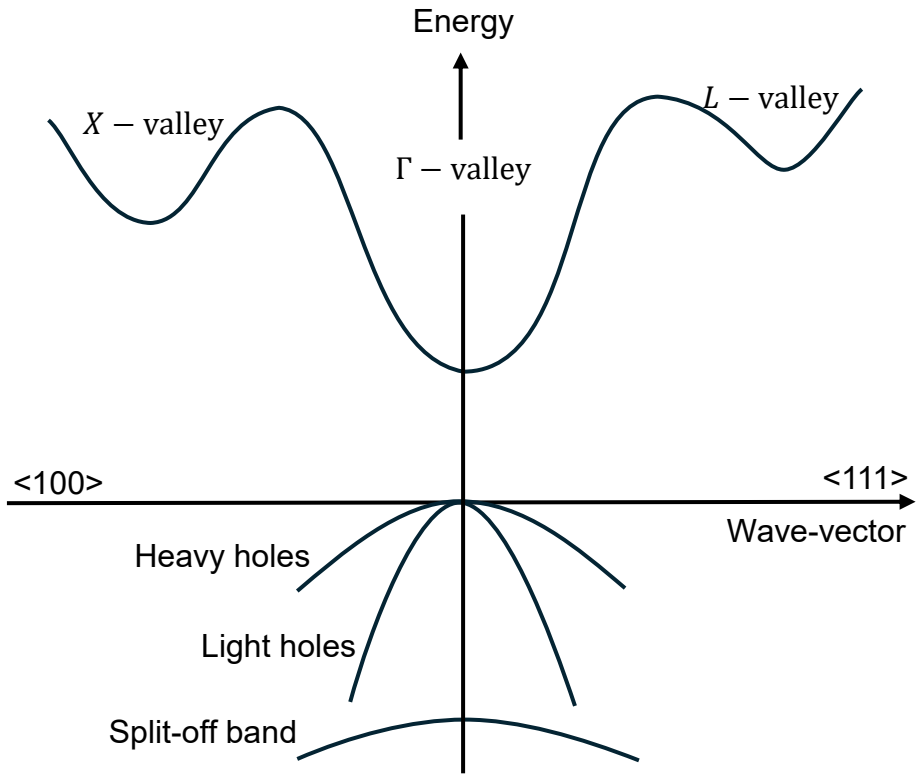

Figure 2.1. *Scheme of a band structure for a direct-band-gap semiconductor. Note how the bands are parabolic in nature: larger curvature leads to a heavier mass, hence the differentiation between heavy and light holes [1].*

not. For a direct-band-gap semiconductor, the minimum energy difference between the valence and conduction band occurs at the Γ-point [1]. An illustrative figure of the band structure for a direct-band-gap semiconductor is depicted in Figure (2.1).

For a ternary compound semiconductor, the band gap depends on the relative composition. The relation between the band gap and composition can be approximated using cubic interpolation [1, 12]

$$E_{\mathrm{g}}(A_xB_{1-x}C) = x \cdot E_{\mathrm{g}}(AC) + (1-x) \cdot E_{\mathrm{g}}(BC) - x(1-x) \cdot C_{\mathrm{g}}, \tag{2.2}$$

where E_{g} is the band gap, x is the composition and C_{g} is the bowing parameter of the ternary semiconductor. Generally, the bowing parameter is also composition-dependent and is unique to the semiconductor [12]. For most common ternary semiconductor alloys, the bowing parameters can be found in literature such as by Vurgaftman et al. [12] or by Adachi et al. [13].

Using band parameters found in literature [12], band gap energies can be graphed for different lattice directions and compositions of AlGaSb. The composition dependence of the band gap for AlGaSb at 12 kelvins is shown in Figure (2.2), although it is important to

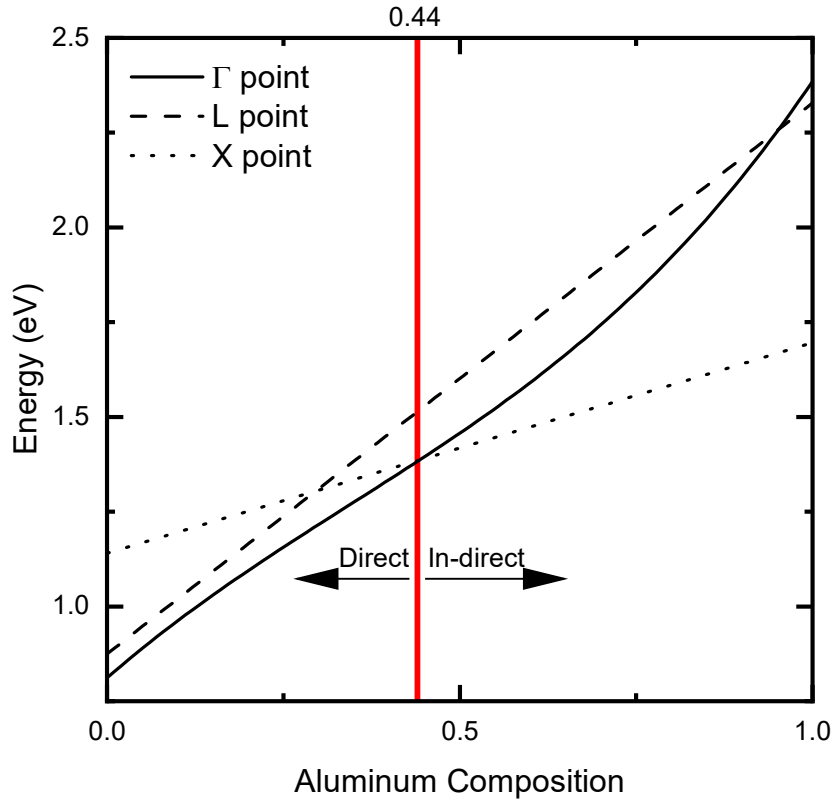

Figure 2.2. *Band gap dependence on composition for AlGaSb at 12 kelvins. Although the switch from direct to indirect occurs at a composition of 0.44, bulk AlGaSb can be tuned on a relatively wide range of wavelengths (from 900 nm to 1520 nm) while still remaining in the direct-band-gap regime.*

note that, at the Γ-point, Vurgaftman provides a composition-dependent bowing parameter, while Adachi provides a constant bowing parameter. As can be seen in Figure (2.2), AlGaSb band gap changes from a direct to an indirect band gap after a composition of $x \approx 0.44$, thus limiting the range of available wavelengths in AlGaSb devices.

The effect of temperature on band structure is also of great interest since most devices are operated in a range of temperatures. At higher temperatures, atoms occupy a larger space, and therefore interactions between atoms are weaker. Consequently, the band gap decreases since less energy is required to form an electron-hole pair (EHP). [14] The band gap dependence on temperature can be estimated using various models, though the most widely used model for semiconductor materials is the empirically deduced Varshni Law [1, 15]

$$E_{\mathrm{g}}(T) = E_{\mathrm{g}}(0) - \frac{AT^2}{B+T}, \tag{2.3}$$

where A and B are experimentally determined parameters which are characteristic of a given semiconductor and T is the temperature of the semiconductor in kelvins. Using the

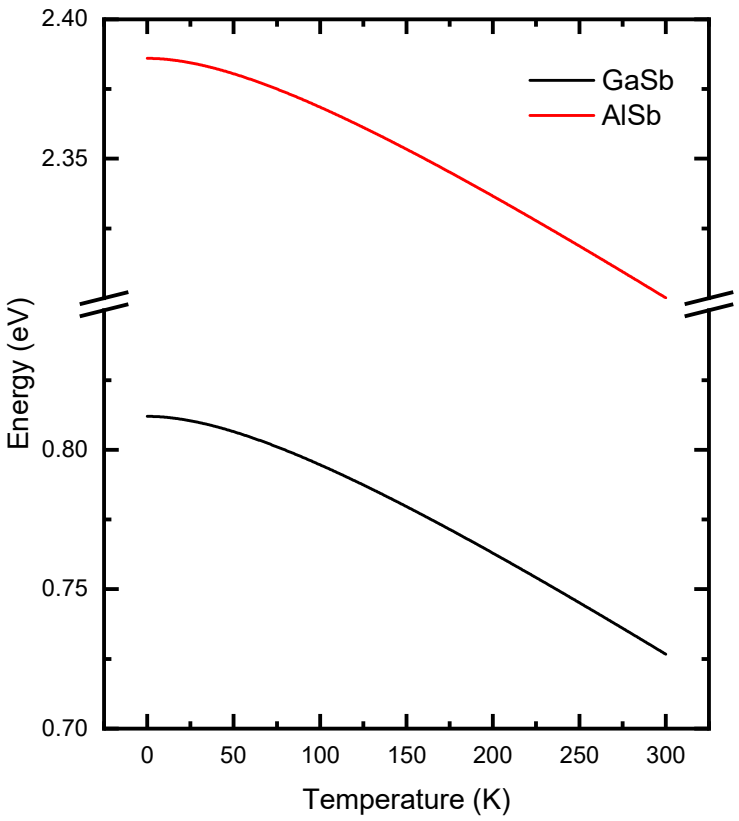

Figure 2.3. *A graph of Varshni law for GaSb and AlSb. At modest temperatures, Varshni law acts linearly. Once cryogenic temperatures are reached, the band gap energy starts to saturate. Parameters used for the calculation from Vurgaftman et al. [12].*

Varshni law in tandem with band structure theory, one may largely account for exciton-phonon interactions within a bulk crystal at low temperatures [16, 17], thus leading to an effective and easy-to-use model. A graph of Varshni law for GaSb and AlSb is shown in figure (2.3).

2.2 Excitons

At low temperatures, the EHP may form a bound state due to attractive Coulomb forces, since the characteristic thermal energy $k_{\mathrm{B}}T$ is lower than the binding energy of the EHP. These bound EHPs are called excitons. There are two types of excitons: 1) Wannier-Mott excitons (free excitons) and 2) Frenkel excitons (tightly bound excitons). Of these two, free excitons are mainly observed in pure semiconductors and are characterized by their long binding radii. [11, 18]

As free excitons consist of a negatively charged electron and a positively charged hole, their energy states in a bulk semiconductor may be described using the free exciton model, which is reminiscent of the hydrogen model [11, 19]

$$E(n) = E_{\mathrm{g}} - \frac{\frac{\mu}{m_0 \epsilon_{\mathrm{r}}^2} \cdot R_{\mathrm{y}}}{n^2} \equiv E_{\mathrm{g}} - \frac{R_{\mathrm{x}}}{n^2}, \tag{2.4}$$

where μ is the reduced mass of the electron-hole pair, m_0 is the free electron mass, ϵ_{r} is the relative permittivity, R_{y} is the Rydberg constant, n is the energy level and R_{x} is the Rydberg energy.

Ultimately, free excitons have an energy lower than the band gap because a part of that energy is bound in the Coulomb interactions between electrons and holes as is described by equation (2.4). This binding energy is in the range of 0.1 meV to 5 meV for III-V semiconductors [19], which is roughly an order of magnitude higher than the characteristic thermal energy at cryogenic temperatures achievable with He-cryostats. For example, the characteristic thermal energy achievable by such a cryostat at 12 kelvins is around 0.1 meV, whereas the binding energy for GaSb is 2.0 meV [11]. Therefore, the binding energy is sufficient to prevent the dissociation of excitons by interaction with acoustic phonons, and free exciton recombination dominates at low temperatures. However, free excitons are not observed in doped semiconductors due to the screening of Coulomb interactions and the ionization of excitons [11, 20].

Although free excitons are not observed in doped semiconductors, Frenkel excitons are observed. Frenkel excitons are localized excitons bound to impurities, such as dopants, and their binding radii are comparable to the interatomic spacing of the crystal. This small radius leads to the collapse of the free exciton model, and therefore other methods, such as TBM, need to be employed in order to solve the Frenkel exciton energies. Furthermore, due to the decrease in radius, the Frenkel exciton binding energy is much larger than the free exciton binding energy. Overall, Frenkel excitons resemble excited atomic states as a result of their localized nature. [18]

2.3 Photoluminescence in Bulk III-V Semiconductors

Photoluminescence occurs when a semiconductor is subjected to an impinging photon flux with a photon energy larger than the band gap of the material. The photons are absorbed as they travel through the semiconductor medium causing electrons to excite onto the conduction band, while simultaneously creating EHPs. These pairs then on average recombine after a carrier lifetime, resulting in emission of photons that correspond to the band gap. [10]

The relation between incident and transmitted photon fluxes is described by the Beer-

Lambert law which states that [1]

$$I = I_0 e^{-\alpha x}, \tag{2.5}$$

where I_0 and I are incident and transmitted photon fluxes, respectively, α is the absorption coefficient and x is the distance traveled through the medium. It is important to note that the absorption coefficient depends on photon energy and that excitons cause sharp absorption peaks near the band edge [10, 11]. Therefore, the transmission of light is more nuanced than is solely described by the Beer-Lambert law.

For a bulk AlGaSb semiconductor, the absorption coefficient can be found in literature for different compositions. For an incident flux of 532 nm, an absorption coefficient of $\alpha = 4.4214 \cdot 10^5\,\mathrm{cm}^{-1}$ is used for an aluminum composition of zero [21]. Using equation (2.5), a 1 µm thick layer of GaSb transmits 64.2 percent, whereas a 1 µm AlGaSb layer with 30 percent aluminum content transmits 64.7 percent of the incident light with an absorption coefficient of $\alpha = 4.3491 \cdot 10^5\,\mathrm{cm}^{-1}$ [21]. Since the absorption is quite modest in both cases, the use of a mirror, such as a distributed Bragg reflector (DBR), may provide a much better absorption of pumping light [10].

Although the band gap energy remains constant, not all emitted photons are of the same energy. Since the difference in energies between the valence and conduction bands depends on where the excited electron is in k-space, the energy of the emitted photon upon recombination also changes in k-space. Thus, the distribution of carriers in k-space largely dictates the emission spectrum for a semiconductor. The carrier distribution, a graph of which can be found in Figure (2.4), is defined by the density of states and Fermi-Dirac statistics. Consequently, the resulting photoluminescence spectrum is somewhat similar to the shape of the carrier distribution. [1, 22]

In addition to the carrier distribution, the emission of light from the semiconductor itself depends on temperature. Since the Fermi-Dirac distribution is temperature dependent, the increase in temperature causes the carriers to shift upward, and therefore a term of $\frac{1}{2}k_{\mathrm{B}}T$ needs to be added to acquire the energy of the photon at peak intensity [10, 11], though the effect of this at cryogenic temperatures is negligible.

2.4 Optical Phonons

In a crystalline structure, such as a zinc-blende structure, atoms oscillate about their lattice points due to thermal energy. This displacement of atoms can perturbate throughout the structure, essentially creating mechanical waves within the material [23]. These waves can be described by quasiparticles, called phonons. A phonon is a descreet unit or quantum of vibrational mechanical energy, and they can be separated into optical and

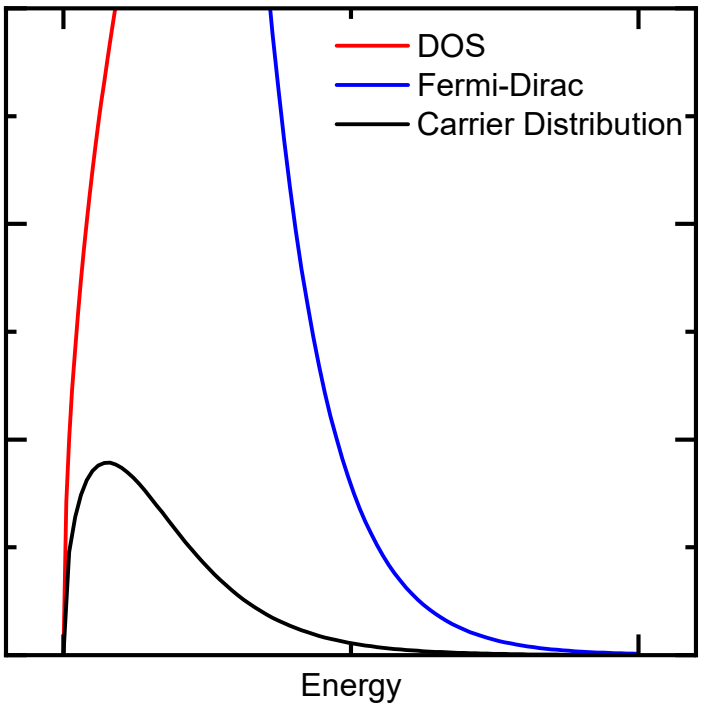

Figure 2.4. *Carrier distribution for a bulk III-V semiconductor. The maximum of the carrier distribution occurs at* $E_{\mathrm{g}} + \frac{1}{2}k_{\mathrm{B}}T$ *[10].*

acoustic phonons. [14] For a zinc-blende crystal, the phonon energies are described by the dispersion relations [24]

$$\omega_{\pm}^2 = K\left(\frac{1}{m_1}+\frac{1}{m_2}\right) \pm K\sqrt{\left(\frac{1}{m_1}+\frac{1}{m_2}\right)^2 - \frac{4\sin^2\left(\frac{ka}{2}\right)}{m_1 m_2}}, \tag{2.6}$$

where ω is the frequency of the mode, K is the spring constant describing the interactions between adjacent atoms, m_1 and m_2 are the masses of two different types of atoms, and a is the lattice constant of the crystal. The minus- and plus-signs are assigned to acoustic and optical phonons, respectively.

Optical phonons can be longitudinal or transversal in a 3-dimensional crystal, depending on the direction of atomic oscillations with respect to the propagation direction of the wave. These three modes (two transverse and one longitudinal) have their own dispersion relations, resulting in six dispersion relations for a III-V bulk semiconductor. An illustrative graph of phonon dispersions for a one-dimensional crystal is presented in Figure (2.5). [23]

Moreover, optical phonons are crucial in LT-PL, since they affect the emission wavelength of photons. In a direct-band-gap semiconductor, exciton relaxation occurs near the Γ-point. When this relaxation occurs, a part of the energy can be transferred to an optical phonon of the same wave-vector. The resulting PL peaks, which originate from radiative

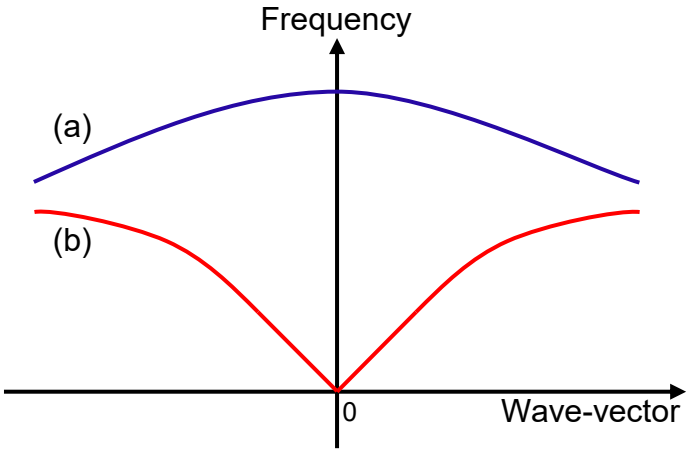

Figure 2.5. *Dispersion relations for (a) acoustic phonons and (b) optical phonons. Acoustic phonons can be seen to have a linear dependence near the Γ-point ($k \approx 0$), whereas the optical phonons remain constant.*

recombination of EHPs involving the participation of optical phonons, are called phonon replicas, and their energies are characteristic of the material. [25, 26] In turn, these energies correspond to a Raman shift, which is defined as [14]

$$\nu = \frac{1}{\lambda_0} - \frac{1}{\lambda_1}, \tag{2.7}$$

where ν is the Raman shift expressed in wavenumber, λ_0 and λ_1 are the wavelengths without and with the emission of a phonon, respectively. Raman shifts for different compositions and modes of AlGaSb are presented in table (2.1). Since the Raman shift corresponding to a phonon replica has an energy of around 10 meV, phonon replicas are only observed at sufficiently low temperatures, further highlighting the importance of cryogenic conditions.

Table 2.1. *Raman shifts for different compositions and modes of AlGaSb. Values were calculated by multiplying Raman shift data by $hc \times 10^{-7}$ m. Original data provided by Ferrini et al. [25]*

$Al_xGa_{1-x}Sb$	$GaSb-$ likemode		$AlSb-$ likemode	
x	E_{TO} (meV)	E_{LO} (meV)	E_{TO} (meV)	E_{LO} (meV)
0.0	28.2	29.2	-	-
0.3	27.7	28.4	39.2	39.8

2.5 Defects

Epitaxial growth of semiconductors always introduces some defects that can be detrimental to the function of the device. They can alter the photoluminescence spectrum [27], cause unwanted heating [28], and restrict the flow of carriers [29]. Defects can be roughly characterized into three categories: 1) Point defects, which can be localized vacancies, impurity atoms, or interstitial atoms, 2) extended defects, which can be line defects such as dislocations, and 3) plane defects, which can be stacking faults or twin planes. [30]

Point defects can be split into two groups. 1) Extrinsic point defects and 2) Intrinsic point defects (also called native defects). Extrinsic point defects refer to impurity atoms at lattice sites that are foreign to the grown crystal. [30] These foreign atoms can be unintentional, such as oxygen in AlGaSb, or intentional, such as tellerium used as a dopant in AlGaSb [31]. On the other hand, intrinsic point defects refer to vacancies (Schottky defects), interstitial atoms (Frenkel defects), or antisites [30]. An antisite is an atom that occupies the wrong sublattice, e.g., a Ga-atom occupying an Sb-atom site is an antisite in GaSb.

The formation of native defects depends on the growth temperature of the grown layer, and the density of native defects can be calculated for Schottky and Frenkel defects in a diatomic lattice. For Schottky defects

$$N_{\mathrm{Schottky}} = N_{\mathrm{lattice}} \exp\left(-\frac{E_{\mathrm{Schottky}}}{2k_{\mathrm{B}}T}\right), \tag{2.8}$$

where N_{lattice} is the density of lattice atoms, E_{Schottky} is the energy required to take a single atom from the crystal volume and place it on the crystal surface, and k_{B} is the Boltzmann constant. For Frenkel defects

$$N_{\mathrm{Frenkel}} = \sqrt{N_{\mathrm{interstitial}} N_{\mathrm{lattice}}} \exp\left(-\frac{E_{\mathrm{Frenkel}}}{2k_{\mathrm{B}}T}\right), \tag{2.9}$$

where $N_{\mathrm{interstitial}}$ is the density of interstitial sites and E_{Frenkel} is the energy needed to take one cation and put it at an interstitial site. [10, 30]

Ultimately, defects create extra states, called trap states, within or outside the band gap. Trap states within the band gap may trap excitons, thus lowering their energy, leading to a lower photoluminescence intensity in the main exciton peak. If the trap state is sufficiently far away from the band gap as to not produce a photon upon the relaxation of an exciton, it is called a deep state. Conversely, if the trap state is close to the valence or conduction band, the trap state is called a shallow state. [14]

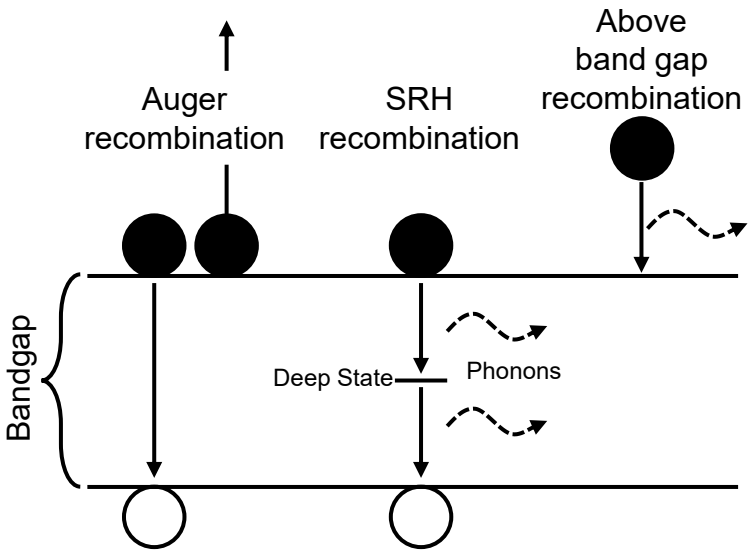

Figure 2.6. *Different non-radiative recombination mechanisms in bulk semiconductors. Note that at low temperature, band gap energy is replaced by exciton energy.*

2.6 Recombination Mechanisms

An exciton has two ways of recombination: non-radiative and radiative emission [1]. These classes can be further divided into subgroups depending on the mechanism through which the recombination occurs. Different non-radiative and radiative recombination mechanisms are illustrated in Figures (2.6) and (2.7).

For non-radiative emission, an exciton can first relax onto a deep state after which it relaxes again, hence releasing two phonons [32]. The mechanism in which an exciton goes through a deep state is called Shockley-Read-Hall recombination [10]. An electron on the conduction band may also give its energy to another electron on the conduction band, and hence relax to the valence band without the emission of a photon. This is called Auger recombination [10]. Lastly, an exciton may be excited above the band gap causing the electron to lose energy through phonon emission. This is called above band gap recombination [9]. Most non-radiative recombination is harmful to the operation of a semiconductor-based device, since non-radiative recombination causes unwanted heating by giving thermal energy via phonons to the lattice. Moreover, non-radiative recombination results in less radiative recombination, further decreasing the quantum efficiency of the semiconductor device. [10] Therefore, identifying and eliminating non-radiative recombination mechanisms is crucial.

Radiative emission, on the other hand, can occur spontaneously, through stimulation, through a trap state, or assisted by a phonon [10, 26]. In spontaneous emission, an exciton recombines directly, emitting a photon in the process. In stimulated emission, another photon stimulates the recombination of an exciton, thus leading to two photons

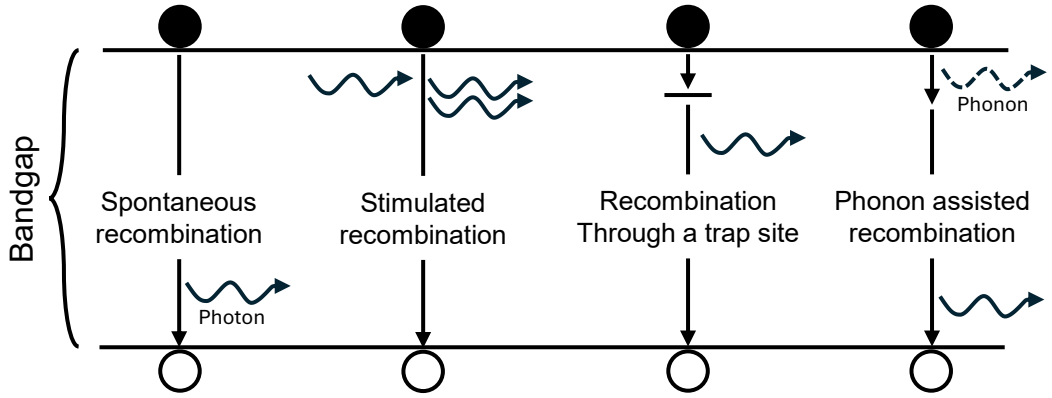

Figure 2.7. *Different radiative recombination mechanisms in bulk semiconductors.*

which are of the same phase [10]. Radiative recombination through a trap state is similar to its non-radiative counterpart, but instead of a deep state, the exciton relaxes through a shallow state, thus leading to a photon of slightly smaller energy [32].

Lastly, a part of the exciton energy may be given to an optical vibrational mode upon relaxation, resulting in phonon replicas [26]. This phenomenon is called phonon-assisted recombination. Because part of the exciton energy is transferred, an emission peak of lower energy and intensity emerges, essentially creating a smaller copy of the original peak but at lower energy. Subsequent phonon replica peak intensities can be modeled using the Hopfield prediction [26]

$$I_n = A \exp\left(-S_n\right) \frac{S^n}{n!}, \tag{2.10}$$

where A is an experimentally determined factor and S is the Huang-Rhys factor. Essentially, the Hopfield prediction tells us that the chance to create an additional phonon replica decreases exponentially. This exponentially decreasing trend is seen in Figure (2.8), where a photoluminescence spectrum of GaAs at 7 K is shown.

As can be seen in the PL spectrum of GaAs, excitons bind to different impurities, causing a shift in the energy of the emitted photons. Left from the main exciton peak is the first impurity peak, corresponding to carbon and its phonon replicas. The carbon ground state is separated by 26.4 meV [33], and the replicas are roughly spaced by 36 meV, which is the energy of a longitudinal optical phonon in GaAs [26, 34]. Going further left in the spectrum, an energy state corresponding to copper impurities arises, separated by 0.15 eV from the main exciton peak [35–37]. The subsequent phonon replica peaks are also roughly separated by 36 meV corresponding to the same longitudinal optical phonons as for the carbon impurities [38].

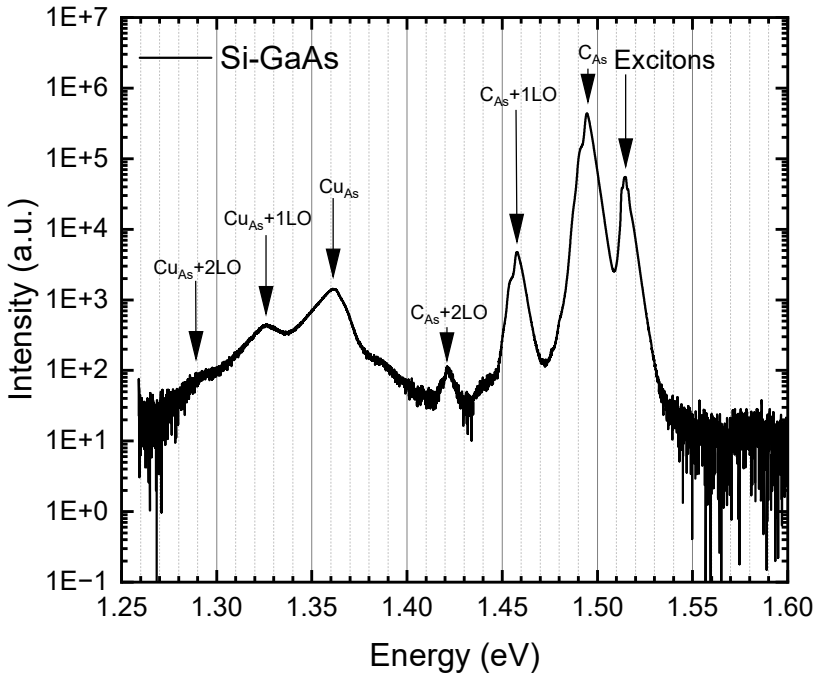

Figure 2.8. *Photoluminescence of GaAs at 7 kelvins. Note that intensity is provided on a logarithmic scale, highlighting the exponentially decreasing probability of subsequent phonon replicas. The notation $C_{As} + 1LO$ means that the peak is the first-order phonon replica of the carbon on arsenide-site defect.*

3. MEASUREMENTS

In this chapter, the LT-PL setup, sample structures, and methodology are discussed. First, the setup is discussed in its entirety covering the devices and pumping wavelengths used in the measurement. Second, the sample structures are presented with descriptions of the functions of the different layers. Finally, the procedure with which the measurement was conducted is conveyed.

3.1 Low Temperature Photoluminescence Measurement Setup

In this study, the LT-PL setup used to conduct the experiment is an optical system that is mounted on a table where each instrument can be adjusted to fit the measurement criteria. The setup consists of the following instruments:

- a PSU-III-FDA 532 nm, or alternatively, a ITC4001 980 nm laser for optical pumping
- an adjustable attenuation filter
- a model SR540 chopper controller connected to a SR830 DSP lock-in amplifier
- a helium-cooled cryostat which contains the sample
- a helium compressor
- a vacuum pump
- focusing lenses
- a 750 nm high-pass filter for 532 nm laser or two 1000 nm high-pass filters for a 980 nm laser in front of a DK480 1/2 monochromator
- a 1000 nm short-pass filter for measuring samples c and d with a 980 nm laser
- a FGA015 or a FD10D indium gallium arsenide photodiode for under 1700 nm or 2600 nm operation respectively

A schematic of the setup is shown in Figure (3.1). Additionally, a 1000 nm short-pass filter was used in tandem with the 980 nm laser in order to eliminate laser emission from the final photoluminescence spectrum.

The samples were carefully mounted onto the stage of the helium-cooled cryostat using tweezers to avoid surface defects from forming. In addition, rubber gloves were used

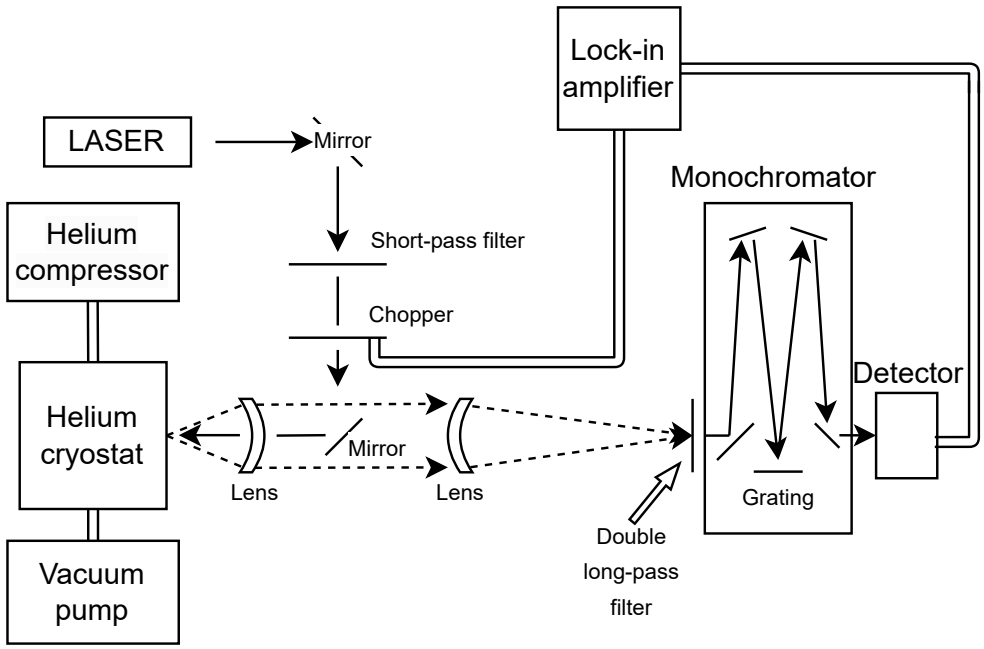

Figure 3.1. *Schematic of the used LT-PL setup. The short-pass filter was used in tandem with the 980 nm laser for the purpose of eliminating additional laser peaks in the PL spectrum. A double long-pass filter was used in front of the monochromator for similar reasons.*

as a protective measure during the mounting process. During the measurement, appropriate protective glasses were used to protect the eyes of the measurer from possible laser reflections, as especially high-power infrared lasers can damage the eyes if directly exposed [39].

Having mounted the sample on the sample stage of the cryostat, the cryostat was closed and then put into the measuring position. Valves connecting the cryostat to the vacuum pump were opened and then the vacuum pump was turned on. Having reached a fan speed of 1500 Hz, the compressor was switched on and the cooling process was started. This took approximately two hours, after which the laser, chopper controller, lock-in amplifier, and power supply of the photodiode were turned on. After the stage and the focusing lenses were aligned so that a maximum photoluminescence intensity was achieved, the measurement was ready to be conducted.

3.2 Samples

In this study, four metamorphically MBE grown samples, the structures of which are shown in Figure (3.2), were measured. The samples had the same base structure except for the GaSb sample, which did not have a superlattice structure. The purpose of this superlattice structure was to act as a DBR, thus providing greater PL intensity. Furthermore, the high band gap of AlSb acted as a barrier for charge carriers, thus reducing

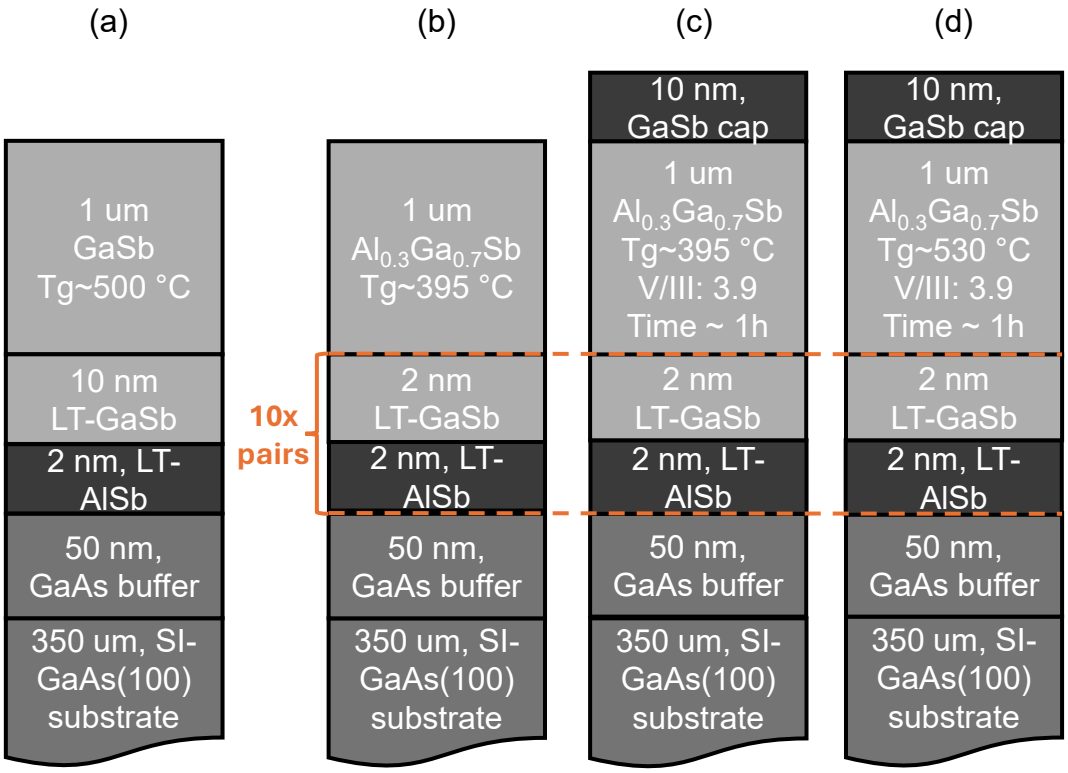

Figure 3.2. *Layer structures of (a) GaSb sample, (b) no-cap AlGaSb sample, (c) low-temperature AlGaSb sample and (d) high-temperature AlGaSb sample. The DBR is made of ten pairs of alternating 2 nm GaSb and AlSb layers.*

carrier leakage from the GaAs buffer.

The top layer was altered for each sample by introducing a capping layer or by changing the growth parameters of the top layer. The capping layer acted as a means to protect the aluminum in the bulk from oxidation, therefore resulting in a clearer PL spectrum. By varying the growth parameters, such as the growth temperature, the defect concentrations could be altered according to equations (2.8) and (2.9).

Moreover, all of the samples were grown on Si-GaAs substrate and had a GaAs buffer layer. This GaAs buffer layer provided a better platform for growing the bulk crystal, thus leading to less defects in the bulk material [40].

3.3 Methodology

PL measurements were made to obtain information on the involvement of impurities and defects. First, the 532 nm laser was aligned with the sample in the cryostat during low-power operation. Since the 532 nm laser was in line with the 980 nm laser, the 980 nm laser was consequently aligned as well. Afterward, two measurements were made on each sample: one with a 532 nm laser and one with a 980 nm laser.

For sample (a), the PL intensities for wavelengths between 1400 nm and 2000 nm were measured, whereas for samples (b) through (d), the PL intensities wavelengths between 1000 nm and 1600 nm were measured. For all samples, the power of the 980 nm laser was 17 mW and the power of the 532 nm laser was 41 mW. The data were then collected in ASCII format and analyzed with Origin 2023b.

4. DATA ANALYSIS

In this chapter, results gathered from the LT-PL measurements are covered. First, possible energy transitions for the GaSb sample are discussed and marked in the LT-PL spectra of the sample. Then, the spectra of the AlGaSb samples are analyzed in the same manner.

4.1 Spectra of the GaSb Sample

Data collected from the LT-PL of sample (a) using a 532 nm and a 980 nm laser was plotted in Figure (4.1). From this figure, a laser emission peak belonging to the second harmonic of the wave (2×980) nm can be observed at around 0.64 eV [41].

Starting from the right, the fundamental band gap of GaSb (in dark yellow) is marked at 812 meV. As can be seen from Figure (4.1), this peak does not fit well into the data, which is expected, since the fundamental transition cannot be observed at cryogenic temperatures due to increased bound exciton recombination. Furthermore, no clear free exciton transition is observed.

Moving to the left, a range of states belonging to the bound states in GaSb [42] are marked from 796 meV to 808.2 meV in pink. From the data it can be seen that there are some faint peaks which might represent these transitions, though this cannot be solely deduced from the LT-PL data.

Marked at 777.8 meV (in blue) is the transition belonging to native defects caused by gallium vacancy-gallium antisite complexes [42]. This transition aligns well with the 532 nm measurement, owing to the higher extinction coefficient of GaSb at 532 nm [21], which results in brighter photoluminescence at shorter wavelengths.

Finally, marked at 706 meV (in dark cyan) is an energy transition corresponding to the singly ionized defect state [43]. This transition cannot be seen from the LT-PL spectrum due to the wide spread of states between 650 meV and 750 meV.

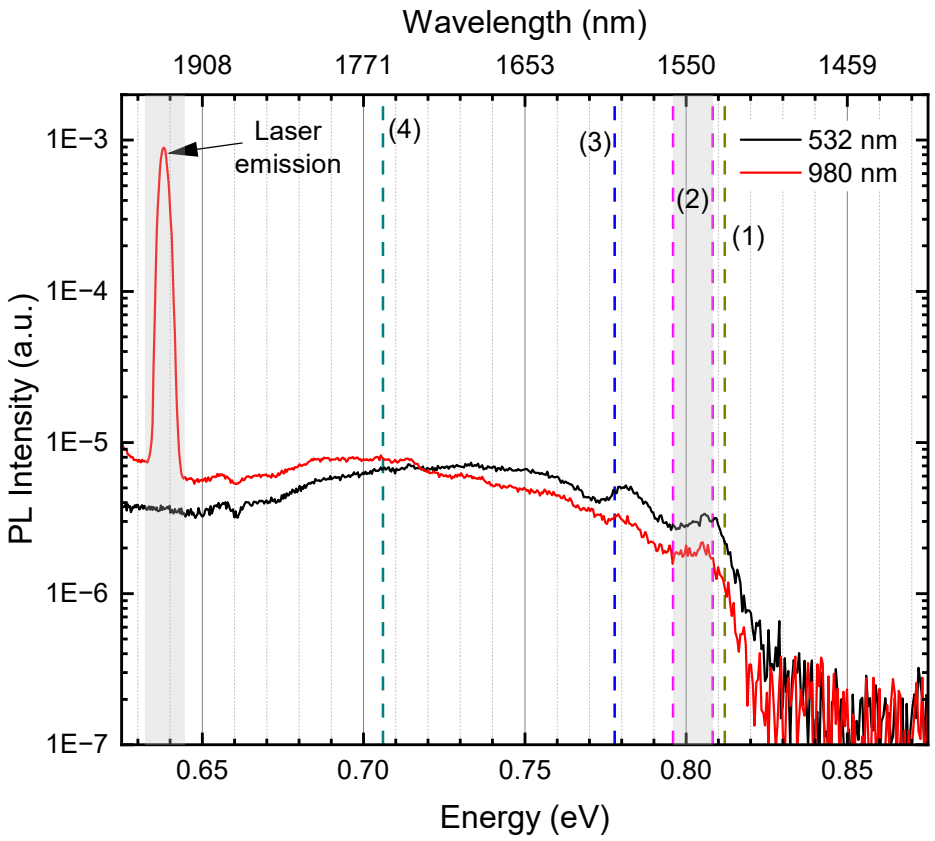

Figure 4.1. *LT-PL spectrum of GaSb measured at 12 kelvins. (1) Fundamental band gap of GaSb, (2) bound exciton states, (3) native lattice defects due to interstitials and antisites, and (4) singly ionized defect state.*

4.2 Spectra of AlGaSb Samples

Data collected from LT-PL of samples (b), (c), and (d) using a 532 nm and a 980 nm laser were plotted in Figure (4.2). From the figure it can be observed that the overall intensity of the 532 nm measurement is lower than that of the 980 nm measurement. This occurs, since the electrons are excited further above the band gap resulting in more above band gap non-radiative recombination, as discussed in Section (2.6).

Starting from the right side of the spectrum in Figure (4.2), the fundamental band gap of $\mathrm{Al_{0.3}Ga_{0.7}Sb}$ at 12 kelvins (in violet) and the free exciton (in magenta), are marked. The free exciton is marked 3 meV below the fundamental band gap of $\mathrm{Al_{0.3}Ga_{0.7}Sb}$ as suggested by Fujita et al. [44]. The fundamental transition and the free exciton cannot be seen in the spectra, since the cryogenic conditions make it more preferable for electron-hole pairs to form bound excitons, as discussed in Section (2.2).

The third marking (in brown) belongs to donor-acceptor native defect state. This state is located 37 meV below the fundamental gap, as suggested by Bignazzi et al. [43].

Although this marking aligns well with the spectra of sample (b), no behaviorally matching LT-PL peaks, which had similar sample structures, were found in literature. Therefore, this peak remains unknown.

Moving to longer wavelengths, the transition energy of a carbon acceptor state in AlSb [45] (in green) is marked, though it is more likely that the state around 1.13 eV is caused by an exciton bound to a native defect (in brown) [42], since the intensity of the peak increases with the growth temperature of the layer, as discussed in Section (2.5).

The GaSb -like mode LO phonon replica of the native defect state (in orange) is marked 28.4 meV below the suspected native defect state at 1.13 meV, as was given in Table (2.1). This marking aligns well with the shoulder of the LT-PL spectrum of sample (d), making it highly likely that this peak is the LO phonon replica of a native defect state.

Marked with a pink dashed line at 1.016 eV is the defect state belonging to oxygen [31]. This mark aligns well with the LT-PL data, and thus it is reasonable to assume that this is indeed an extrinsic defect state caused by oxygen. Furthermore, oxygen concentration seems to decrease with growth temperature, which is in agreement with the findings of Schmult et al. [46] and Giulian et al. [47]. A two-peak fit to the LT-PL data of sample (b) at around 1.00 eV reveals that these transitions, possibly belonging to oxygen, have energies of 1.00 eV and 0.99 eV. Moreover, a dim PL peak at 1.02 eV can be identified from the 532 nm measurement of sample (d). This peak is highly likely associated with the decrease in oxygen concentration as a result of higher growth temperatures.

Lastly, the fundamental band gap of GaSb at 12 kelvins (in dark yellow) is marked at 0.812 eV. From the 532 nm laser measurement, it can be seen that the actual photoluminescence from GaSb occurs roughly around 0.850 eV owing to the quantization of energy states in the top GaSb layer due to low thickness [1, 10]. Moreover, due to the absence of a capping layer, this peak is missing from sample (b), further confirming that this peak belongs to a semi-quantized energy transition. On the other hand, it can be seen that the 980 nm measurement provides less intensity. This is because GaSb has a higher extinction coefficient at 532 nm [21], thus leading to more recombination in the capping layer, as discussed in Section (2.6).

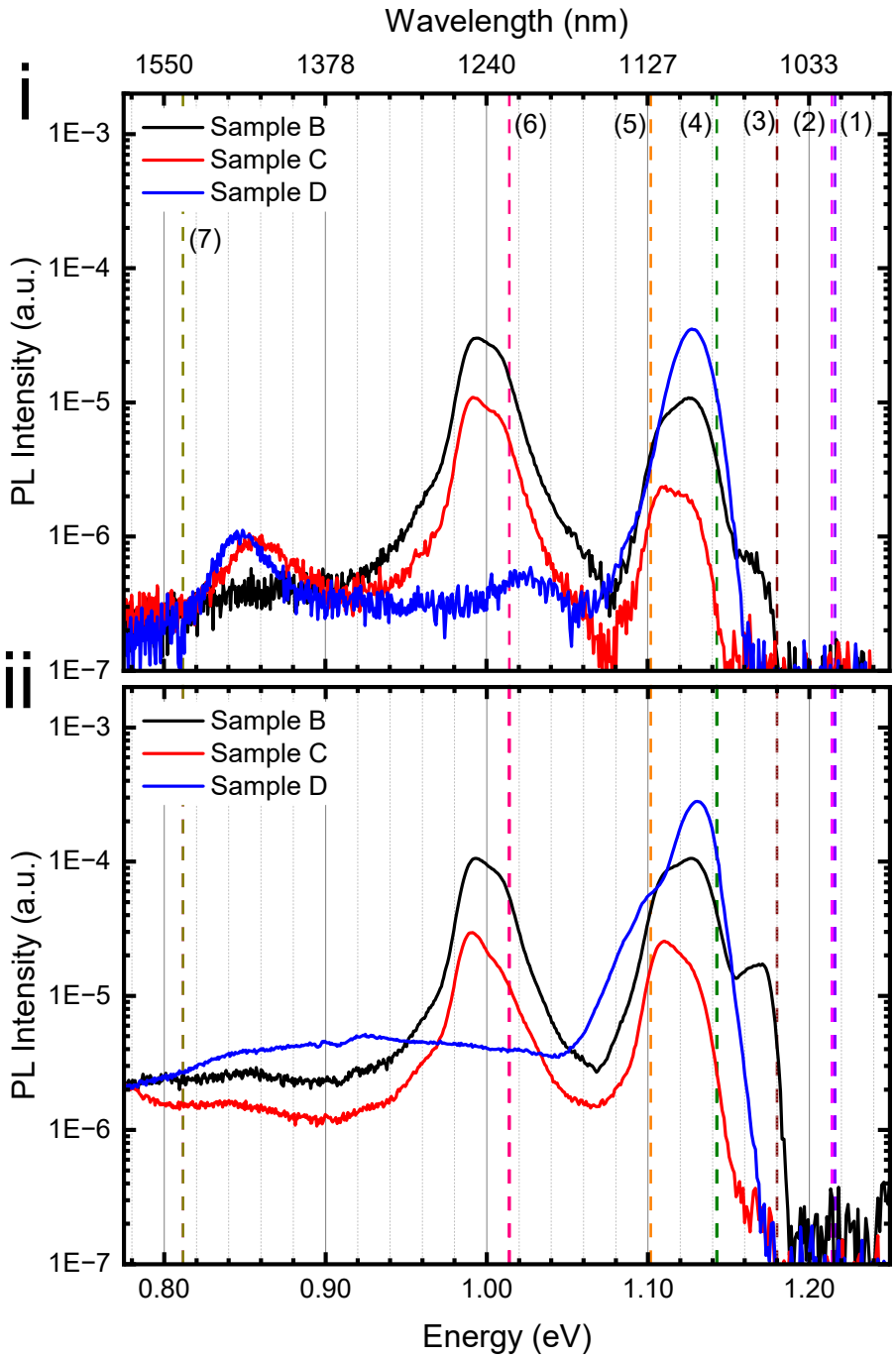

Figure 4.2. *LT-PL spectrum of $Al_{0.3}Ga_{0.7}Sb$ measured at 12 kelvins. (i) and (ii) are measurements done with 532 nm laser and 980 nm laser, respectively. (1) Fundamental band gap of $Al_{0.3}Ga_{0.7}Sb$, (2) free exciton, (3) donor-acceptor native defect state [43], (4) carbon acceptor state (5) GaSb -like mode LO phonon replica of the native defect state at 1.13 eV (6) $O_{Sb}(C_{3v})$ defect state, and (7) fundamental band gap of GaSb. The overall intensity of the 532 nm laser measurement appears lower due to increased above band gap non-radiative recombination.*

5. CONCLUSION

In this thesis, possible transitions in GaSb and $\mathrm{Al_{0.3}Ga_{0.7}Sb}$ were identified from the LT-PL spectra of different samples. These transitions were then put into context, giving insight into the possible effects the sample structures have on the LT-PL. Furthermore, the effect of oxygen and native defects on the LT-PL of these structures was realized.

This thesis started by introducing important concepts in LT-PL. First, the formation of band structure in III-V semiconductors according to TBM was discussed, after which the effects on band gap caused by lattice orientation, sample composition, and temperature were explored. Moreover, this influence on band gap was demonstrated using a composition model and the Varshni Law, providing more information about the effects of these parameters. After utilizing these models, the effects of excitons, optical phonons, and defects on LT-PL were assessed. Their nature in the LT-PL spectra of a Si-GaAs sample was analyzed by taking into consideration the different recombination mechanisms they cause. Finally, the influence of cryogenic temperatures was realized through the observation of phonon replicas at low temperatures and the absence of them at modest temperatures.

From the LT-PL spectra of the GaSb sample, bound exciton states from 796 meV to 808.2 meV and native lattice defects at 777.8 meV were observed. In the case of the $\mathrm{Al_{0.3}Ga_{0.7}Sb}$ samples, emission peaks belonging to native defects at 1.13 eV, GaSb - like mode LO phonon replica of the native defect state at 1.1016 eV, oxygen defect states at 1.016 eV and GaSb emission at 0.850 eV were observed.

From the identification of different transition peaks in LT-PL, the effect of defects on the spectra was realized. Most notably, the effect of oxygen on $\mathrm{Al_{0.3}Ga_{0.7}Sb}$ was greatly impacted by growth temperature, highlighting the importance of proper growth conditions. Furthermore, native defects had a substantial effect on the spectra: they showed high-intensity PL peaks, and their intensity increased with growth temperature, which was expected based on the theory of native defects. From these observations, it can be concluded that the increase in growth temperature results in the rise of the native defect concentration and the fall of oxygen concentration.

Although the measurement was standardized, there were a few sources of possible error in the measurements of the samples. First, the temperature of the cryogenic chamber

was not steady; rather it would oscillate between 12 and 14 kelvins. The effect of such a small temperature fluctuation is still negligible considering that the energy difference is only a fraction of the exciton binding energy in GaSb. Another source of error was the sample surface. Debris, such as dust, and other surface deformations due to handling of the sample, may have a great impact on the received intensity from the samples, although this cannot be shown without surface analysis methods.

Future research may focus on what the hole and electron concentrations were in the samples, as well as what kind of surface structures the samples had. For these purposes, hall measurements and surface analyzing methods, such as X-ray diffraction (XRD), would be suitable options. The hall measurements would give an idea of the native defect concentrations (given compensation effects are minimal), further confirming the increase in concentration due to increased growth temperature. XRD, on the other hand, would give insight into the quality of the surface and whether that had a substantial impact on the intensity or not. Future research may also consider growing the bulk material at an intermediate temperature. This would further confirm the concentration-increasing trend the native defects have.

REFERENCES

[1] Ben G Streetman and Sanjay Banerjee. *Solid state electronic devices*. Seventht edition, Global edition. Boston: Pearson, 2016. ISBN: 1-292-06055-7.

[2] Farseem M. Mohammedy and M. Jamal Deen. “Growth and fabrication issues of GaSb-based detectors”. In: *Journal of Materials Science: Materials in Electronics* 20.11 (Nov. 2009), pp. 1039–1058. ISSN: 1573-482X. DOI: 10.1007/s10854-009-9927-y. URL: https://doi.org/10.1007/s10854-009-9927-y.

[3] Miya T. et al. “Ultimate low-loss single-mode fibre at 1.55 µm”. In: *Electronics Letters* 15.4 (Feb. 1979). Publisher: The Institution of Engineering and Technology, pp. 106–108. DOI: 10.1049/el:19790077. URL: https://doi.org/10.1049/el:19790077 (visited on 03/21/2025).

[4] Nouman Zia et al. “Widely tunable 2 µm hybrid laser using GaSb semiconductor optical amplifiers and a Si3N4 photonics integrated reflector”. In: *Optics Letters* 48.5 (Mar. 2023). Publisher: Optica Publishing Group, pp. 1319–1322. DOI: 10.1364/OL.480867. URL: https://opg.optica.org/ol/abstract.cfm?URI=ol-48-5-1319.

[5] Brian Bennett et al. “Antimonide-based compound semiconductors for electronic devices: A review”. In: *Solid-State Electronics* 49 (Dec. 2005), pp. 1875–1895. DOI: 10.1016/j.sse.2005.09.008.

[6] J.C. Woo et al., eds. *Compound Semiconductors 2004*. en. 0th ed. CRC Press, Apr. 2005. ISBN: 978-1-4822-6922-2. DOI: 10.1201/9781482269222. URL: https://www.taylorfrancis.com/books/9781482269222 (visited on 03/21/2025).

[7] Hideyuki Toyota et al. “Growth and characterization of GaSb/AlGaSb multi-quantum well structures on Si (001) substrates”. In: *Journal of Crystal Growth* 310.1 (Jan. 2008), pp. 78–82. ISSN: 0022-0248. DOI: 10.1016/j.jcrysgro.2007.10.008. URL: https://www.sciencedirect.com/science/article/pii/S0022024807008597.

[8] Primavera Lopez-Salazar et al. “Relaxation and tilting of single and double layer structures of AlGaSb/GaSb-LPE studied by high resolution x-ray diffraction”. In: *Materials Research Express* 7 (Mar. 2020). DOI: 10.1088/2053-1591/ab78c9.

[9] Jasprit Singh. *Electronic and optoelectronic properties of semiconductor structures*. Electronic & optoelectronic properties of semiconductor structures. Cambridge: Cambridge University Press, 2003. ISBN: 978-0-511-07863-7.

[10] Joachim Piprek. *Semiconductor Optoelectronic Devices: Introduction to Physics and Simulation*. 1st ed. Chantilly: Elsevier Science & Technology, 2003. ISBN: 0-12-557190-9. DOI: 10.1016/C2009-0-22633-X.

[11] Mark Fox. *Optical properties of solids*. Second edition. Oxford master series in physics ; 3. Condensed matter physics. Oxford ; Oxford University Press, 2010. ISBN: 978-0-19-157672-0.

[12] I. Vurgaftman, J. R. Meyer, and L. R. Ram-Mohan. “Band parameters for III–V compound semiconductors and their alloys”. In: *Journal of Applied Physics* 89.11 (June 2001), pp. 5815–5875. ISSN: 0021-8979. DOI: 10.1063/1.1368156. URL: https://doi.org/10.1063/1.1368156 (visited on 04/11/2024).

[13] Sadao Adachi. “III-V Ternary and Quaternary Compounds”. In: *Springer Handbook of Electronic and Photonic Materials*. Ed. by Safa Kasap and Peter Capper. Cham: Springer International Publishing, 2017, pp. 1–1. ISBN: 978-3-319-48933-9. DOI: 10.1007/978-3-319-48933-9_30. URL: https://doi.org/10.1007/978-3-319-48933-9_30.

[14] Karl W Böer and Udo W Pohl. *Semiconductor Physics*. 1st ed. 2018. Cham: Springer International Publishing AG, 2018. ISBN: 978-3-319-69148-0. DOI: 10.1007/978-3-319-69150-3.

[15] Y.P. Varshni. “Temperature dependence of the energy gap in semiconductors”. In: *Physica* 34.1 (Jan. 1967), pp. 149–154. ISSN: 0031-8914. DOI: 10.1016/0031-8914(67)90062-6. URL: https://www.sciencedirect.com/science/article/pii/0031891467900626.

[16] Prashant K Sarswat and Michael L Free. “A study of energy band gap versus temperature for Cu2ZnSnS4 thin films”. In: *Physica B: Condensed Matter* 407.1 (2012). Publisher: Elsevier, pp. 108–111. ISSN: 0921-4526.

[17] Kevin O’Donnell and X. Chen. “Temperature Dependence of Semiconductor Band Gaps”. In: *Applied Physics Letters* 58 (July 1991), pp. 2924–2926. DOI: 10.1063/1.104723.

[18] Karl W. Böer and Udo W. Pohl. “Excitons”. In: *Semiconductor Physics*. Ed. by Karl W. Böer and Udo W. Pohl. Cham: Springer International Publishing, 2023, pp. 529–591. ISBN: 978-3-031-18286-0. DOI: 10.1007/978-3-031-18286-0_14. URL: https://doi.org/10.1007/978-3-031-18286-0_14.

[19] B.P. Zakharchenya and S.A. Permogorov. “Excitons in Crystals”. In: *Encyclopedia of Condensed Matter Physics*. Ed. by Franco Bassani, Gerald L. Liedl, and Peter Wyder. Oxford: Elsevier, Jan. 2005, pp. 171–179. ISBN: 978-0-12-369401-0. DOI: 10.1016/B0-12-369401-9/01147-5. URL: https://www.sciencedirect.com/science/article/pii/B0123694019011475.

[20] J. G. Gay. “Screening of Excitons in Semiconductors”. In: *Physical Review B* 4.8 (Oct. 1971). Publisher: American Physical Society, pp. 2567–2575. DOI: 10.1103/PhysRevB.4.2567. URL: https://link.aps.org/doi/10.1103/PhysRevB.4.2567.

[21] R. Ferrini, M. Patrini, and S. Franchi. “Optical functions from 0.02 to 6 eV of AlxGa1−xSb/GaSb epitaxial layers”. In: *Journal of Applied Physics* 84.8 (Oct. 1998), pp. 4517–4524.

ISSN: 0021-8979. DOI: 10.1063/1.368677. URL: https://doi.org/10.1063/1.368677 (visited on 01/21/2025).

[22] Randy Harris. *Modern physics*. Pearson Education, Aug. 2013. ISBN: 978-1-292-03643-4.

[23] Stephen J. Blundell and Katherine M. Blundell. *Concepts in Thermal Physics*. Oxford University Press, Oct. 2009. ISBN: 978-0-19-956209-1. DOI: 10.1093/acprof:oso/9780199562091.001.0001. URL: https://doi.org/10.1093/acprof:oso/9780199562091.001.0001 (visited on 01/30/2025).

[24] P. Misra. *Physics of Condensed Matter*. Elsevier Science, 2011. ISBN: 978-0-12-384954-0. URL: https://books.google.fi/books?id=VV80IAEACAAJ.

[25] Rolando Ferrini et al. "Phonon response of AlxGa1-xSb/GaSb epitaxial layers by Fourier-transform infrared-reflectance and Raman spectroscopies". In: *Phys. Rev. B* 56 (Sept. 1997). DOI: 10.1103/PhysRevB.56.7549.

[26] P. Altieri et al. "Competition in the carrier capture between InGaAs/AlGaAs quantum dots and deep point defects". In: *Physics of Condensed Matter* 28 (July 2002), pp. 157–161. DOI: 10.1140/epjb/e2002-00217-7.

[27] N. Segercrantz et al. "Point defect balance in epitaxial GaSb". In: *Applied Physics Letters* 105.8 (Aug. 2014), p. 082113. ISSN: 0003-6951. DOI: 10.1063/1.4894473. URL: https://doi.org/10.1063/1.4894473 (visited on 01/11/2024).

[28] J.W. Pomeroy et al. "Thermal mapping of defects in AlGaN/GaN heterostructure field-effect transistors using micro-Raman spectroscopy". In: *Applied Physics Letters* 87.10 (2005). DOI: 10.1063/1.2041823. URL: https://www.scopus.com/inward/record.uri?eid=2-s2.0-24644483096&doi=10.1063%2f1.2041823&partnerID=40&md5=335481a06590c6677638b787a09d6209.

[29] J.P. Braga et al. "The role of intrinsic trap states in the semiconductor/insulating interface on the electrical performance of spray-coated thin-film transistors". In: *Materials Science in Semiconductor Processing* 151 (2022). DOI: 10.1016/j.mssp.2022.106984. URL: https://www.scopus.com/inward/record.uri?eid=2-s2.0-85135387757&doi=10.1016%2fj.mssp.2022.106984&partnerID=40&md5=4c18a6cba174318afd45765456006c0f.

[30] Karl W. Böer and Udo W. Pohl. "Crystal Defects". In: *Semiconductor Physics*. Ed. by Karl W. Böer and Udo W. Pohl. Cham: Springer International Publishing, 2018, pp. 529–579. ISBN: 978-3-319-69150-3. DOI: 10.1007/978-3-319-69150-3_15. URL: https://doi.org/10.1007/978-3-319-69150-3_15.

[31] Paul Erhart, Daniel Åberg, and Vincenzo Lordi. "Extrinsic point defects in aluminum antimonide". In: *Physical Review B* 81.19 (May 2010). Publisher: American Physical Society, p. 195216. DOI: 10.1103/PhysRevB.81.195216. URL: https://link.aps.org/doi/10.1103/PhysRevB.81.195216.

[32] B. K. Meyer. "Bound Exciton Complexes". In: *Zinc Oxide: From Fundamental Properties Towards Novel Applications*. Ed. by Claus F. Klingshirn et al. Berlin, Heidel-

berg: Springer Berlin Heidelberg, 2010, pp. 169–199. ISBN: 978-3-642-10577-7. DOI: 10.1007/978-3-642-10577-7_7. URL: https://doi.org/10.1007/978-3-642-10577-7_7.

[33] Tobias Henksmeier et al. “Molecular beam epitaxy growth and temperature-dependent electrical characterization of carbon-doped GaAs on GaAs(1 1 1)B”. In: *Journal of Crystal Growth* 512 (Apr. 2019), pp. 164–168. ISSN: 0022-0248. DOI: 10.1016/j.jcrysgro.2019.02.006. URL: https://www.sciencedirect.com/science/article/pii/S0022024819300806.

[34] Masashi Ozeki et al. “Photoluminescence Study of Carbon Doped Gallium Arsenide”. In: *Japanese Journal of Applied Physics* 13.7 (July 1974), p. 1121. ISSN: 1347-4065. DOI: 10.1143/JJAP.13.1121. URL: https://dx.doi.org/10.1143/JJAP.13.1121.

[35] C. S. Fuller, K. B. Wolfstirn, and H. W. Allison. “DEFECTS IN GaAs PRODUCED BY COPPER”. In: *Applied Physics Letters* 4.3 (Feb. 1964), pp. 48–49. ISSN: 0003-6951. DOI: 10.1063/1.1753957. URL: https://doi.org/10.1063/1.1753957 (visited on 01/29/2025).

[36] J. M. Whelan and C. S. Fuller. “Precipitation of Copper in Gallium Arsenide”. In: *Journal of Applied Physics* 31.8 (Aug. 1960), pp. 1507–1508. ISSN: 0021-8979. DOI: 10.1063/1.1735880. URL: https://doi.org/10.1063/1.1735880 (visited on 01/29/2025).

[37] Richard H. Bube and Harold E. MacDonald. “Temperature Dependence of Photo-Hall Effects in High-Resistivity Gallium Arsenide. II. Two-Carrier Effects”. In: *Physical Review* 128.5 (Dec. 1962). Publisher: American Physical Society, pp. 2071–2077. DOI: 10.1103/PhysRev.128.2071. URL: https://link.aps.org/doi/10.1103/PhysRev.128.2071.

[38] K. K. Tiong et al. “Effects of As+ ion implantation on the Raman spectra of GaAs: “Spatial correlation” interpretation”. In: *Applied Physics Letters* 44.1 (Jan. 1984), pp. 122–124. ISSN: 0003-6951. DOI: 10.1063/1.94541. URL: https://doi.org/10.1063/1.94541 (visited on 01/29/2025).

[39] Yaniv Barkana and Michael Belkin. “Laser Eye Injuries”. In: *Survey of Ophthalmology* 44.6 (May 2000), pp. 459–478. ISSN: 0039-6257. DOI: 10.1016/S0039-6257(00)00112-0. URL: https://www.sciencedirect.com/science/article/pii/S0039625700001120.

[40] Mohamed. Henini. *Molecular beam epitaxy : from research to mass production*. 1st ed. Amsterdam: Elsevier, 2012. ISBN: 978-1-283-73426-4.

[41] Maosheng He and Jeffrey M. Forbes. “Rossby wave second harmonic generation observed in the middle atmosphere”. In: *Nature Communications* 13.1 (Dec. 2022), p. 7544. ISSN: 2041-1723. DOI: 10.1038/s41467-022-35142-3. URL: https://doi.org/10.1038/s41467-022-35142-3.

[42] Wen-Jang Jiang, Yuh-Maoh Sun, and Meng-Chyi Wu. “Electrical and photoluminescent properties of high-quality GaSb and AlGaSb layers grown from Sb-rich solutions by liquid-phase epitaxy”. In: *Journal of Applied Physics* 77.4 (Feb. 1995), pp. 1725–1728. ISSN: 0021-8979. DOI: 10.1063/1.359576. URL: https://doi.org/10.1063/1.359576 (visited on 03/20/2025).

[43] A. Bignazzi et al. “Low temperature photoluminescence of tellurium-doped GaSb grown by molecular beam epitaxy”. In: *Journal of Crystal Growth* 169.3 (Dec. 1996), pp. 450–456. ISSN: 0022-0248. DOI: 10.1016/S0022-0248(96)00441-1. URL: https://www.sciencedirect.com/science/article/pii/S0022024896004411.

[44] S. Fujita et al. “LOW-TEMPERATURE GROWTH CONDITIONS AND PROPERTIES OF AlGa (As) Sb ON GaSb SUBSTRATE BY LPE”. In: *Le Journal de Physique Colloques* 43.C5 (Dec. 1982), pp. C5–29–C5–38. ISSN: 0449-1947. DOI: 10.1051/jphyscol:1982505. URL: http://www.edpsciences.org/10.1051/jphyscol:1982505 (visited on 03/20/2025).

[45] M. D. McCluskey, E. E. Haller, and P. Becla. “Carbon acceptors and carbon-hydrogen complexes in AlSb”. In: *Physical Review B* 65.4 (Dec. 2001). Publisher: American Physical Society, p. 045201. DOI: 10.1103/PhysRevB.65.045201. URL: https://link.aps.org/doi/10.1103/PhysRevB.65.045201.

[46] S. Schmult et al. “Control of unintentional oxygen incorporation in GaN”. In: *Journal of Vacuum Science and Technology B: Nanotechnology and Microelectronics* 35.2 (2017). DOI: 10.1116/1.4975925. URL: https://www.scopus.com/inward/record.uri?eid=2-s2.0-85012898782&doi=10.1116%2f1.4975925&partnerID=40&md5=776857d0adb61cf6cbda685ec577f816.

[47] R. Giulian et al. “Structural and electronic characterization of antimonide films made by magnetron sputtering”. In: *Journal of Physics D: Applied Physics* 50.7 (2017). DOI: 10.1088/1361-6463/aa5368. URL: https://www.scopus.com/inward/record.uri?eid=2-s2.0-85011295989&doi=10.1088%2f1361-6463%2faa5368&partnerID=40&md5=80be5130f8d40a31136538b4f6430fa6.